

Article

3D-QSAR, ADME-Tox In Silico Prediction and Molecular Docking Studies for Modeling the Analgesic Activity against Neuropathic Pain of Novel NR2B-Selective NMDA Receptor Antagonists

Mohamed El fadili ^{1,*}, Mohammed Er-rajy ¹, Hamada Imtara ^{2,*}, Mohammed Kara ³, Sara Zarougui ¹, Najla Altwaijry ⁴, Omkulthom Al kamaly ⁴, Aisha Al Sfouk ⁴ and Menana Elhallaoui ¹

- ¹ Engineering Materials, Modeling and Environmental Laboratory, Faculty of Sciences Dhar El Mehraz, Sidi Mohammed Ben Abdellah University, BP 1796 Atlas, Fez 30000, Morocco; er.rajy@usmba.ac.ma (M.E.-r.); sara.zarougui@usmba.ac.ma (S.Z.); menana.elhallaoui@usmba.ac.ma (M.E.)
- ² Faculty of Arts and Sciences, Arab American University Palestine, P.O. Box 240, Jenin 44862, Palestine
- ³ Laboratory of Biotechnology, Conservation and Valorisation of Naturals Resources, Faculty of Sciences Dhar El Mehraz, Sidi Mohamed Ben Abdellah University, BP 1796 Atlas, Fez 30000, Morocco; mohammed.kara@usmba.ac.ma
- ⁴ Department of Pharmaceutical Sciences, College of Pharmacy, Princess Nourah bint Abdulrahman University, P.O. Box 84428, Riyadh 11671, Saudi Arabia; najla.altwaijry@usmba.ac.ma (N.A.); omalkmali@pnu.edu.sa (O.M.A.k.); aisha.sfouk@usmba.ac.ma (A.A.S.)
- * Correspondence: mohamed.elfadili@usmba.ac.ma (M.E.f.); hamada.tarayrah@gmail.com (H.I.)



Citation: El fadili, M.; Er-rajy, M.; Imtara, H.; Kara, M.; Zarougui, S.; Altwaijry, N.; Al kamaly, O.; Al Sfouk, A.; Elhallaoui, M. 3D-QSAR, ADME-Tox In Silico Prediction and Molecular Docking Studies for Modeling the Analgesic Activity against Neuropathic Pain of Novel NR2B-Selective NMDA Receptor Antagonists. *Processes* **2022**, *10*, 1462. <https://doi.org/10.3390/pr10081462>

Academic Editor: Jaime Yáñez

Received: 26 June 2022

Accepted: 20 July 2022

Published: 26 July 2022

Publisher's Note: MDPI stays neutral with regard to jurisdictional claims in published maps and institutional affiliations.



Copyright: © 2022 by the authors. Licensee MDPI, Basel, Switzerland. This article is an open access article distributed under the terms and conditions of the Creative Commons Attribution (CC BY) license (<https://creativecommons.org/licenses/by/4.0/>).

Abstract: A new class of selective antagonists of the N-Methyl-D-Aspartate (NMDA) receptor subunit 2B have been developed using molecular modeling techniques. The three-dimensional quantitative structure–activity relationship (3D-QSAR) study, based on comparative molecular field analysis (CoMFA) and comparative molecular similarity index analysis (CoMSIA) models, indicate that steric, electrostatic and hydrogen bond acceptor fields have a key function in the analgesic activity against neuropathic pain. The predictive accuracy of the developed CoMFA model ($Q^2 = 0.540$, $R^2 = 0.980$, $R^2_{pred} = 0.613$) and the best CoMSIA model ($Q^2 = 0.665$, $R^2 = 0.916$, $R^2_{pred} = 0.701$) has been successfully examined through external and internal validation. Based on ADMET in silico properties, L1, L2 and L3 ligands are non-toxic inhibitors of 1A2, 2C19 and 2C9 cytochromes, predicted to passively cross the blood–brain barrier (BBB) and have the highest probability to penetrate the central nervous system (CNS). Molecular docking results indicate that the active ligands (L1, L2 and L3) interact specifically with Phe176, Glu235, Glu236, Gln110, Asp136 and Glu178 amino acids of the transport protein encoded as 3QEL. Therefore, they could be used as analgesic drugs for the treatment of neuropathic pain.

Keywords: 3D-QSAR; ADMET; neuropathic pain; analgesic activity; molecular docking; NMDA

1. Introduction

Chronic pain is one of the most frequent reasons for medical consultations [1], and can be considered as a critical cause of morbidity and disability [2]. For this reason, a variety of analgesics have been designed to treat chronic pain, such as opioids, antidepressants, anticonvulsants, and nonsteroidal anti-inflammatory drugs (NSAIDs) [3]. However, opioid analgesic (OA) treatment of chronic pain remains controversial, its efficacy is unclear, and it has been associated with undesirable secondary effects [4], similar to those of morphine, such as constipation, nausea, vomiting, pruritus, drowsiness, cognitive impairment, respiratory depression, tolerance, physical dependence and addiction [3,5]. Consequently, the search for new potent non-opioid analgesics (NOA), more effective on the central nervous system (CNS), is an absolute priority [3] because they are highly desired in medical practice [6]. In this regard, the pain control is a world health problem, indicating an

ever-increasing need for the discovery of new molecules with better analgesic activity and reduced secondary effects [7]. For this purpose, novel isoxazole, piperidine linker moieties, and phenylpiperazine derivatives, illustrated in Figure 1, show potential as analgesic drugs, and have been introduced to treat these types of acute and chronic diseases, reacting similar to selective antagonists of the N-Methyl-D-Aspartate (NMDA) receptor subunit 2B that inhibit the binding of [3H]-ifenprodil to brain membranes and do not cause side effects associated with non-selective N-Methyl-D-Aspartate receptor antagonists [8]. NMDA receptors are ligand-gated cationic channels expressed in brain tissue and naturally activated by the simultaneous action of glutamate and glycine [9]; in addition, they are required for both brain development and many higher order functions [10]. At the same time, they can cause the death of neurons as a result of receptor hyperactivation [9]. Consequently, NMDA receptors are considered as high profile therapeutic targets in the treatment of pain and neurodegenerative diseases such as Alzheimer's, Huntington's and Parkinson's disease [11]. The present study is conducted using three-dimensional quantitative structure activity relationships (3D-QSARs) a commonly used technology to discover new drugs, identifying high affinity ligands for a targeted protein [12,13]. The robustness, predictability and reliability of the established CoMFA and CoMSIA models have been examined with the help of a cross validation technique for the training set (26 molecules), and external validation for the test set (6 molecules), as a crucial and decisive step to judge the prediction accuracy of the constructed model for a novel database [14,15]. During the second part, we predicted ADMET in silico properties [16] of 32 molecules compared to a co-crystallized ligand (ifenprodil) as an anti-hypertensive agent, with neuroprotective activity through its effects on N-Methyl-D-Aspartate (NMDA) receptors [17], based on the BOILED-Egg predictive model and Lipinski, Ghose, Muegge, Veber and Egan rules. Lastly, the predicted inhibitors (L1, L2 and L3) were chosen for molecular docking simulations to study their intermolecular interactions towards the active sites of the protein target encoded as 3QEL [18], and this approach has been validated using docking validation protocol [19].

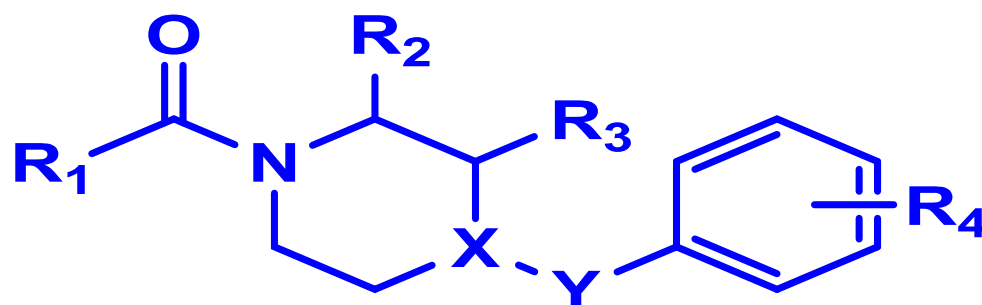


Figure 1. Structural formula of isoxazole (1–6), piperidine linker moieties (6–14) and phenylpiperazine (12, 15–32) derivatives.

2. Materials and Methods

2.1. Experimental Database

To establish the 3D-QSAR models, we selected a set of 32 compounds from the recently published work of Anan, K et al., including NR2B-selective antagonists that inhibit the binding of [3H]-ifenprodil to rat brain membranes [8], as summarized in Figure 1. Then, we randomly divided this complete set into two subsets: the first one (training set) included 26 compounds that were used to build the model, and the second one (test set) included 6 compounds to validate the established model, as marked in Table 1.

Table 1. The studied compounds and their observed activities of pIC₅₀ order.

| Compounds | R ₁ | R ₂ | R ₃ | R ₄ | X | Y | pIC ₅₀ (bind) |
|-----------|----------------|----------------|----------------|--------------------|----|-----------------|--------------------------|
| 1 | | H | H | H | CH | CH ₂ | 7.1 |
| 2 | | H | H | 4-F | CH | CH ₂ | 7.1 |
| 3 | | H | H | 4-Cl | CH | CH ₂ | 7.2 |
| 4 | | H | H | H | CH | CH ₂ | 7.2 |
| 5 | | H | H | 4-F | CH | CH ₂ | 7.3 |
| 6 | | H | H | 4-Cl | CH | CH ₂ | 7.6 |
| 7 | | H | H | 4-F | CH | CH ₂ | 7.5 |
| 8 | | H | H | 4-Cl | N | CH ₂ | 6 |
| 9 * | | H | H | 4-Cl | N | None | 6 |
| 10 | | H | H | 4-Cl | CH | CH ₂ | 7.5 |
| 11 | | H | H | 4-Cl | N | CH ₂ | 6.3 |
| 12 * | | H | H | 4-Cl | N | None | 7.8 |
| 13 | | H | H | 4-Cl | N | None | 6 |
| 14 | | H | H | 4-Cl | N | None | 6 |
| 15 | | H | H | H | N | None | 6 |
| 16 * | | H | H | 4-F | N | None | 6.9 |
| 17 * | | H | H | 4-CF ₃ | N | None | 7.6 |
| 18 | | H | H | 4-OCH ₃ | N | None | 6.6 |
| 19 | | H | H | 3,4-2F | N | None | 7.7 |
| 20 | | H | H | 3,5-2F | N | None | 6.8 |

Table 1. Cont.

| Compounds | R ₁ | R ₂ | R ₃ | R ₄ | X | Y | pIC ₅₀ (bind) |
|-----------|----------------|--------------------------|--------------------------|------------------------|---|------|--------------------------|
| 21 | | H | H | 3-Cl,4-F | N | None | 7.5 |
| 22 | | H | H | 3-F,4-Cl | N | None | 7.9 |
| 23 | | H | H | 3-F,4-CF ₃ | N | None | 7.8 |
| 24 * | | H | H | 3-F,4-OCH ₃ | N | None | 7.8 |
| 25 | | CH ₃ backward | H | 4-Cl | N | None | 7.5 |
| 26 | | CH ₃ forward | H | 4-Cl | N | None | 6 |
| 27 | | H | CH ₃ backward | 4-Cl | N | None | 7.2 |
| 28 | | H | CH ₃ forward | 4-Cl | N | None | 6.2 |
| 29 * | | CH ₃ backward | H | 3,4-2F | N | None | 7.3 |
| 30 | | H | CH ₃ backward | 3,4-2F | N | None | 7.2 |
| 31 | | CH ₃ backward | H | 3-F,4-Cl | N | None | 7.9 |
| 32 | | H | CH ₃ backward | 3-F,4-Cl | N | None | 7.3 |

* indicates test set molecules.

2.2. Optimisation and Alignment

With the assistance of SYBYL-X 2.0 software (Tripos, Inc., St. Louis, MO, United States of America USA), we first constructed the thirty-two molecules, which were optimized using the Tripos force fields and Gasteiger–Huckel atomic partial charges. Then, the convergence parameter of the Powell gradient algorithm was specified to be 0.001 kcal/(mol.Å), with a maximum of 10,000 iterations to guarantee the conformational stability for each molecular system by making the energies in Kcal/mol completely minimized [20–22]. In the second stage, we aligned the set of molecules as one of the most significant steps to ensure the robustness of the CoMFA and CoMSIA models [23,24].

2.3. Development of 3D-QSAR Models

3D-QSAR models were generated via CoMFA and CoMSIA studies, using the partial least squares (PLS) analysis [25,26], where the steric and electrostatic fields of the CoMFA model were produced with a default energy cutoff of 30 kcal/mol. The attenuation factor and column filtering were defined as default values of 0.3 and 2.0 kcal/mol, respectively. Moreover, many additional physico-chemical descriptors, such as the hydrogen bond acceptor (HBA), hydrogen bond donor (HBD) and hydrophobic fields, were additionally calculated for the CoMSIA model in the identical conditions. A total of sixteen various

combinations of fields were considered to develop the best CoMSIA model, as shown in Table 2.

Table 2. The statistical results of CoMFA and CoMSIA models in various molecular field combinations using partial least squares analysis.

| | Q^2 | R^2 | SEE | F | ONC | R^2_{pr} | Fractions | | | | |
|--------------|-------|-------|-------|---------|-------|------------|-----------|---------------|-------------|-------|----------|
| | | | | | | | Steric | Electrostatic | Hydrophobic | Donor | Acceptor |
| CoMFA | 0.540 | 0.980 | 0.110 | 124.198 | 7 | 0.613 | 0.857 | 0.143 | - | - | - |
| CoMSIA/SEA | 0.667 | 0.903 | 0.228 | 37.421 | 5 | 0.420 | 0.304 | 0.524 | - | - | 0.172 |
| CoMSIA/SEH | 0.592 | 0.821 | 0.296 | 33.700 | 3 | 0.110 | 0.141 | 0.221 | 0.638 | - | - |
| CoMSIA/SED | 0.704 | 0.908 | 0.218 | 51.754 | 4 | 0.465 | 0.399 | 0.601 | - | 0 | - |
| CoMSIA/SHD | 0.537 | 0.755 | 0.347 | 22.618 | 3 | 0.131 | 0.204 | - | 0.796 | 0 | - |
| CoMSIA/SHA | 0.568 | 0.763 | 0.341 | 23.641 | 3 | 0.015 | 0.161 | - | 0.678 | - | 0.161 |
| CoMSIA/SDA | 0.320 | 0.564 | 0.462 | 9.505 | 3 | 0.522 | 0.5 | - | - | 0 | 0.5 |
| CoMSIA/EHA | 0.617 | 0.817 | 0.300 | 32.718 | 3 | 0.018 | - | 0.209 | 0.634 | - | 0.157 |
| CoMSIA/EHD | 0.579 | 0.756 | 0.338 | 35.624 | 2 | 0.010 | - | 0.211 | 0.789 | 0 | - |
| CoMSIA/EDA | 0.665 | 0.916 | 0.238 | 19.365 | 9 | 0.701 | - | 0.627 | - | 0 | 0.373 |
| CoMSIA/HDA | 0.546 | 0.762 | 0.342 | 23.449 | 3 | 0.025 | - | - | 0.801 | 0 | 0.199 |
| CoMSIA/EHDA | 0.617 | 0.817 | 0.300 | 32.718 | 3 | 0.018 | - | 0.209 | 0.634 | 0 | 0.157 |
| CoMSIA/SHDA | 0.568 | 0.763 | 0.341 | 23.641 | 3 | 0.015 | 0.161 | - | 0.678 | 0 | 0.161 |
| CoMSIA/SEDA | 0.667 | 0.903 | 0.228 | 37.421 | 5 | 0.420 | 0.304 | 0.524 | - | 0 | 0.172 |
| CoMSIA/SEHA | 0.620 | 0.808 | 0.307 | 30.844 | 3 | 0.007 | 0.122 | 0.172 | 0.568 | - | 0.138 |
| CoMSIA/SEHD | 0.592 | 0.821 | 0.296 | 33.700 | 3 | 0.110 | 0.141 | 0.221 | 0.638 | 0 | - |
| CoMSIA/SEHDA | 0.620 | 0.808 | 0.307 | 30.844 | 3 | 0.007 | 0.122 | 0.172 | 0.568 | 0 | 0.138 |

Abbreviations: Q^2 : the cross-validation determination coefficient, R^2 : the non-cross-validation determination coefficient, SEE : the standard estimation error, F : the Fischer test value, ONC : the optimum number of components, and R^2_{pr} : the external validation determination coefficient.

2.4. Partial Least Squares (PLS) Analysis

To model the linear relationship between a set of structural predictors and the response variable (analgesic activity of pIC_{50} order) with a good quality of adjustment and a good predictive power [27,28], we have applied the partial least squares regression (PLSR) technology, with the help of SYBYL-X 2.0 software. The cross-validated determination coefficient (Q^2) for an optimum number of principal components (ONC) was calculated using the leave-one-out (LOO) procedure, and the non-cross-validated determination coefficient (R^2), F -test value and the standard estimation error (SEE) were calculated using the non-cross validation procedure. Where the best 3D-QSAR model was based on the optimum values of Q^2 , R^2 must be greater than 0.5 and 0.6 [29,30] for the optimum number of components (ONC) and lowest standard error of estimation (SEE), respectively. To examine the reliability of the generated model, which was developed on 26 molecules (training set), we performed the external validation technique, using the 'predict' function included in the SYBYL package. Then, based on the previously developed model which was saved in sln format, we predicted the analgesic activities of pIC_{50} order for 6 novel molecules (test set), as illustrated in Table 3. The required condition: $R^2_{ext} > 0.6$ was verified afterwards using Excelstat software [31].

Table 3. The results of external validation corresponding to CoMFA and CoMSIA/EDA models.

| Compounds Number | Observed pIC_{50} | Predicted pIC_{50} of CoMFA | Predicted pIC_{50} of CoMSIA/EDA |
|------------------|---------------------|-------------------------------|------------------------------------|
| 9 * | 6 | 8.2 | 6.7 |
| 12 * | 7.8 | 9.6 | 7.3 |
| 16 * | 6.9 | 9.7 | 7.4 |
| 17 * | 7.6 | 10.0 | 7.4 |
| 24 * | 7.8 | 10.2 | 7.4 |
| 29 * | 7.3 | 10.6 | 7.5 |

* Indicates the test set molecules.

2.5. ADMET In Silico Pharmacokinetics

To identify the new drug with a high success level and reduced experimental study duration, it is mandatory to examine the absorption, distribution, metabolism, excretion and toxicity (ADMET) of these substances in the human organism before beginning the investigative process. [32,33], satisfying a few basic rules including Lipinski's [34], Veber's [35], Ghose's [36], Egan's [37,38] and Muegge's [39] regulations. This technology is equally applicable to remove the substances with potentially unfavorable physiological features, considering the pharmacokinetic qualities and toxicity [40]. For this purpose, we evaluated pharmacokinetic in silico characteristics of novel tested compounds as analgesic drugs against neuropathic pain, through the use of SwissADMET [41] and pkCSM [42] online servers, respectively.

2.6. Molecular Docking Modeling

Molecular docking is often used in computational chemistry to accelerate drug discovery at early stages. For this project, the molecular modeling technique was based on the cell key phenomenon, where the best position of the ligand or drug candidate (the agent) is the key that can open the cell (or protein) to finally have a more stable complex by energetic order [43]. We started this study by extracting the protein responsible for the GluN2B subunit [44], coded as 3QEL.pdb from the protein data bank file [17], discovered by the X-ray diffraction method, in machine simulation with a resolution equal to 2.60 Å [45]. Then, we performed the dissolution, removing all the water molecules bound to the protein; then we deleted the sodium atom and the suspended ligands, while adding the polar hydrogens using the discovery studio software, for the reason that the cavity method works best [46]. After the preparation of the protein and quoting its active sites, we launched the docking calculation in AutoDock 4.2 software [47]. With the help of algorithm AUTOGRID, we were able to centralize the grid box, putting the sizes 100, 100, and 100 in its three-dimensional structure with a spacing of 0.375 Å, and executing ten genetic algorithms, for a sum of 2,500,000 evals. Finally, we obtained the strongest complex out of the fifty obtained conformations [48], and we visualized 3D and 2D interactions of the protein–ligand with the use of discovery studio 2021 [49].

3. Results and Discussion

3.1. Molecular Alignment

To ensure the reliability and accuracy of CoMFA and CoMSIA models, the three-dimensional molecular structures of test and training sets were completely minimized and then aligned on the most active compound (molecule 22), which was selected as the template. *N,N*-diethylacetamide is the common core resulting from the superposition of the molecules on the template, as displayed in the Figure 2.

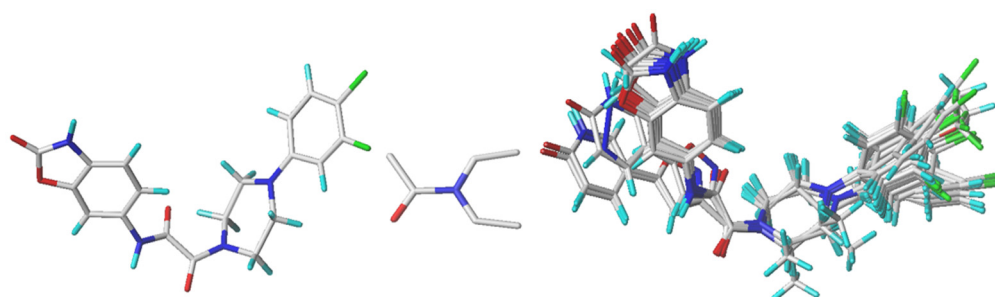


Figure 2. 3D structure of the molecule 22 as template (left), 32 aligned and superposed molecules on the template (right) and the common core (middle).

3.2. 3D-QSAR Analysis

The present 3D-QSAR study was performed using comparative molecular field analysis (CoMFA) and comparative molecular similarity index analysis (CoMSIA) as two classical

methods used to investigate the quantitative correlations between 3D molecular descriptors and inhibitory activity [50]. The statistical results presented in Table 2 indicate that the CoMFA model obtained for an optimum number of principal components ($ONC = 7$) using the partial least squares analysis is given by an excellent non-cross-validated determination coefficient $R^2 = 0.98$ (much higher than 0.6), a good cross-validated determination coefficient Q^2_{cv} of 0.540, a high predictive value for the external validation of test set R^2_{pred} of 0.613, with a minimal standard estimation error SEE of 0.110 and F -test value of 124.198. According to the Golbraikh and Tropsha study, the established model is efficient and robust, because it has been successfully validated using the external validation performed for the test set (R^2_{pred} superior than 0.6), and the internal validation performed for the training test with the help of cross-validation technique (Q^2_{cv} superior than 0.5) [30]. Therefore, the CoMFA analysis indicates that the biological activity of the pIC_{50} order is affected by steric and electrostatic fields with a contribution rate of 85.7% and 14.3%, respectively. Moreover, we developed 16 various models from the comparative molecular similarity index analysis (CoMSIA), which included five three-dimensional descriptors, such as steric (S), electrostatic (E), hydrogen bond acceptor (HBA or A), hydrogen bond donor (HBD or D) and hydrophobic (H) fields; however, only the CoMSIA/EDA model was validated using internal and external validation. This mathematical model was produced for an optimum number of components ($ONC = 9$) using the partial least squares analysis, and given by a very good non-cross-validated determination coefficient $R^2 = 0.916$ (much higher than 0.6), a good cross-validated determination coefficient Q^2_{cv} of 0.665, and a high predictive value for the external validation of test set R^2_{pred} of 0.701, with a minimal standard estimation error SEE of 0.238 and an F -test value of 19.365. Although the Golbraikh and Tropsha statistical criteria were verified, the non-cross-validated determination coefficient (R^2), the cross-validated determination coefficient (Q^2_{cv}) and the external validation of test set (R^2_{pred}) were greater than 0.6, 0.5 and 0.6 respectively; as such, the CoMSIA/EDA model was successfully validated, indicating that electrostatic and hydrogen bond acceptor fields have a key function in the analgesic activity against chronic pain, with a contribution rate of 62.7% and 37.3%, respectively.

3.3. A Graphical Explanation of CoMSIA/EDA and CoMFA Models

The structural features influencing the development of biological activity were visualized using the contour maps of the 3D-QSAR models [51], as shown in Figure 3, where the compound 22 structure was chosen as a reference. The green contours displayed in Figure 3A, contributing 80%, indicate the regions where bulky clusters can enhance the biological activity, while the yellow contours, contributing 20%, indicate the regions where bulky clusters decrease the activity. Moreover, 80% of favorable contribution of the electrostatic field is expressed by the blue contours, and 20% of unfavorable contribution of the electrostatic field is represented by the red contours, as illustrated in the Figure 3B. In addition, the magenta-colored contour maps with 80% contribution indicate the hydrogen bond acceptor field that reinforces the activity, while the red contours of 20% contribution indicate the disadvantaged region, as shown in Figure 3C. We have noted the absence of the hydrogen bond donor (HBD) field, as shown in Figure 3D, since the results presented in Table 2 confirm no impact of HBD in the CoMSIA models; therefore, steric (A), electrostatic (B) and hydrogen bond acceptor (C) fields are the main factors that influenced the biological activity. Additionally, we observed a green contour in meta and para positions, especially for the isoxazole derivatives, indicating that the selection of the voluminous substitution group in this area is necessary to make the ligand more active. Moreover, we detected a blue contour in the same disubstituted aromatic cycle in the meta and para positions, which makes the molecule most active. We also discovered, in the reverse part of the template molecule, a very important magenta contour in the [Oxazol-2(3H)-one] group, explaining the high activity of the inhibitor.

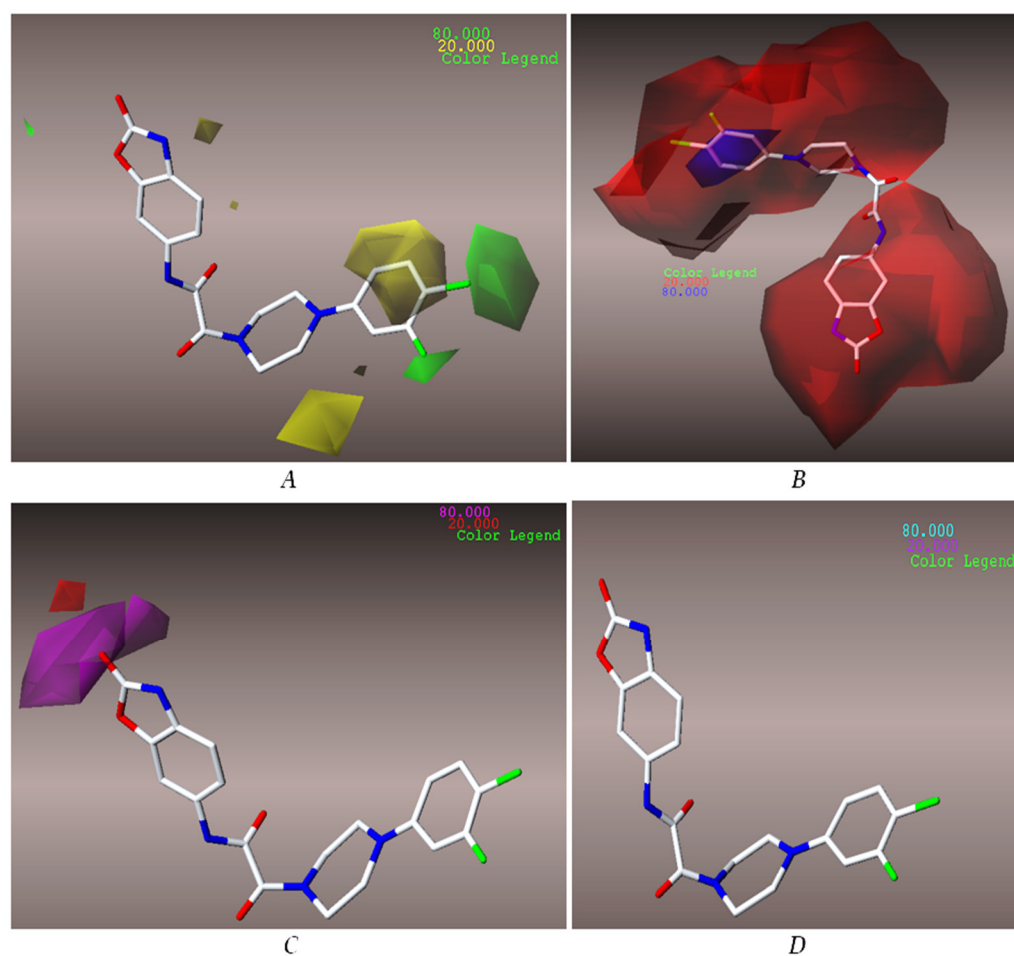


Figure 3. Std*coeff. contour maps corresponding to steric (A), electrostatic (B), hydrogen bond acceptor (C) and hydrogen bond donor (D) fields explained for the compound 22 as a template.

3.4. ADMET In Silico Pharmacokinetics

Based on ifenprodil as an anti-hypertensive agent, with neuroprotective activity through its effects on N-Methyl-D-Aspartate (NMDA) receptors [17], we have tested the thirty-two molecules using BOILED-Egg as an accurate and reliable predictive model. This model is strongly applicable in the context of medicinal chemistry and drug discovery, focused on the evolution of lipophilicity, defined by the logarithm of the partition coefficient between n-octanol and water solvents (LogP O/W) in the Y-axis, as a function of polarity, given by the topological polar surface area (TPSA) in the X-axis [52]. Figure 4 presents only the L1, L2 and L3 ligands that are part of the yellow Egan Egg, due to the fact that they have a TPSA inferior to 80 \AA^2 ; as such, they are the inhibitors with the greatest ability to cross the blood–brain barrier (BBB). In contrast, the other 29 molecules, which are part of the white egg zone, are most likely to be absorbed from the gastrointestinal tract [53]. Consequently L1, L2 and L3 inhibitors, as well as ifenprodil as a co-crystallized ligand, were further examined using adsorption, distribution, metabolism, excretion and toxicity (ADMET) pharmacokinetic parameters on the basis of Lipinski, Veber, Egan, Muegge and Ghose rules [33,54]. Compared to ifenprodil, the results successively presented in the Tables 4 and 5 clearly illustrate that the three inhibitors respect the Lipinski thresholds, and satisfy the favorable violation numbers of Veber, Egan, Muegge and Ghose without exception. Moreover, they have efficient absorption at the level of human intestine (IAH over 89%), and a significant distribution, due to the fact that their volumes of distribution in humans are intended to be superior to -0.44 Log L/kg . At the blood–brain barrier (BBB), their permeabilities are significantly higher than -1 Log BB , except for the ligand L3. At

the level of the central nervous system (CNS), they have permeabilities outside the (−2 to −3 Log PS) range, so they all access the central nervous system (CNS). In addition, they are all predicted to be inhibitors of the 1A2, 2C19 and 2C9 cytochromes; however, ifenprodil has been predicted to be an inhibitor of 1A2 and 2D6 cytochromes. Consequently, L1, L2 and L3 ligands are engineered as non-poisonous operators for the central nervous system (CNS), because of their high potential to cross the blood–brain barrier (BBB).

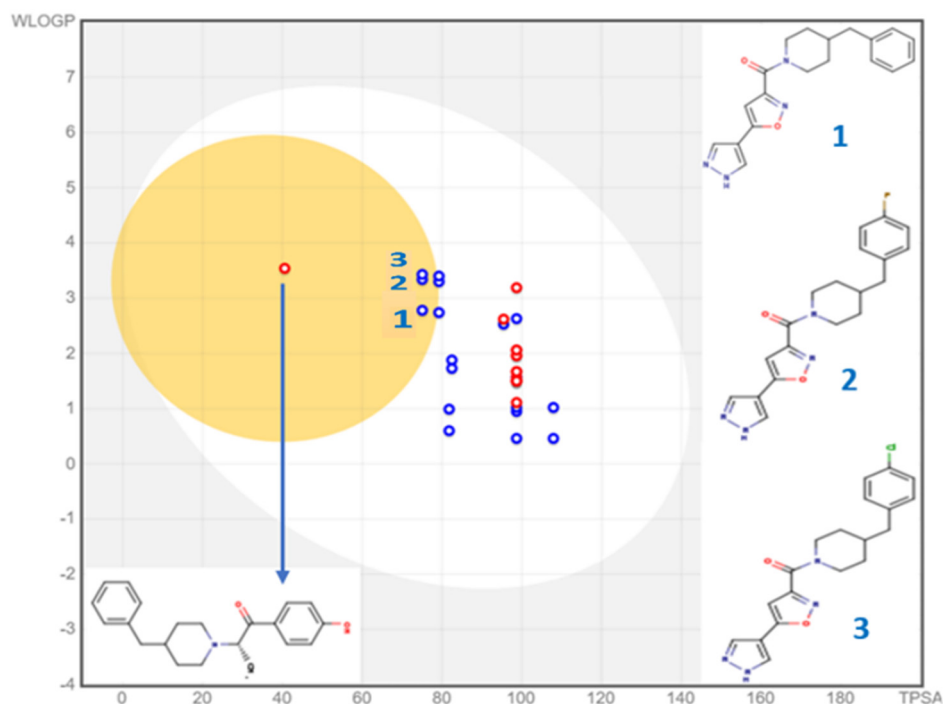


Figure 4. BOILED-Egg predictive model of the co-crystallized ligand and the thirty-two inhibitors.

Table 4. Physicochemical parameters prediction of ifenprodil, L1, L2 and L3 ligands on the basis of Lipinski, Veber, Egan, Muegge and Ghose regulations.

| Physical and Chemical Properties | | | | | | | Lipinski Violations | Veber Violations | Egan Violations | Ghose Violations | Muegge Violations |
|----------------------------------|--------------------------------|--------------------------------|------------------------------|----------------------------|---------------------------------|----------------------------|------------------------|---------------------|--------------------|---------------------|----------------------|
| Ligands number | Molecular weight (g/mol) | Molar re- fractive index | Rotatable bonds Number | Log P (Oc- tanol/Water) | Hydrogen bond ac- ceptors | H-bond donors Number | | | | | |
| Threshold | ≤500 | $40 \leq MR \leq 130$ | <10 | <5 | ≤10 | <5 | Yes/No | Yes/No | Yes/No | Yes/No | Yes/No |
| L1 | 336.39 | 97.50 | 5 | 2.26 | 4 | 1 | Yes | Yes | Yes | Yes | Yes |
| L2 | 354.38 | 97.46 | 5 | 2.41 | 5 | 1 | Yes | Yes | Yes | Yes | Yes |
| L3 | 370.83 | 102.51 | 5 | 2.53 | 4 | 1 | Yes | Yes | Yes | Yes | Yes |
| Ifenprodil | 323.43 | 101.49 | 5 | 3.47 | 3 | 1 | Yes | Yes | Yes | Yes | Yes |

Table 5. ADMET properties prediction of ifenprodil, L1, L2 and L3 ligands.

| Ligands number | Absorption | | Distribution | | Metabolism | | | | | | Excretion | Toxicity | |
|-------------------------|-------------------------------------|---------------------|-----------------------|-----------------------|------------|-----|-----------|------|-----|-----|-----------------|----------------------------|-------------------------|
| | Intestinal Absorption (human) | VDss (human) | BBB per- meability | CNS per- meability | Substrate | | Inhibitor | | | | Total Clearance | AMES toxicity | |
| | | | | | 2D6 | 3A4 | CYP | | | | | | |
| | | | | | | | 1A2 | 2C19 | 2C9 | 2D6 | | | 3A4 |
| Numeric (% Absorbed) | Numeric (Log L/kg) | Numeric (Log BB) | Numeric (Log PS) | Categorical (Yes/No) | | | | | | | | Numeric (Log mL/min/kg) | Categorical (Yes/No) |
| L1 | 94.525 | 0.191 | −0.965 | −2.361 | Yes | Yes | Yes | Yes | Yes | No | Yes | 0.264 | Not toxic |
| L2 | 89.981 | 0.346 | −0.176 | −2.53 | No | Yes | Yes | Yes | Yes | No | No | 0.197 | Not toxic |
| L3 | 89.079 | 0.475 | −1.138 | −2.376 | No | Yes | Yes | Yes | Yes | No | No | 0.156 | Not toxic |
| Ifenprodil | 92.417 | 1.23 | 0.046 | −1.079 | Yes | Yes | Yes | No | No | Yes | No | 0.993 | Not toxic |

3.5. Molecular Docking

The results of molecular docking were concentrated on the transport protein of 3QEL.pdb connected to ifenprodil as a novel N-Methyl-D-Aspartate (NMDA) receptor antagonist that selectively inhibits receptors, including the NR2B subunit [55]. The crystal structure of this receptor was extracted from the protein data base (PDB) through the use of the X-ray diffraction process at a reasonable resolution equal to 2.6 Å [17,56]. Thus, the results of the intermolecular interactions established between L1, L2 and L3 ligands and the 3QEL encoded protein were compared to experimentally produced intermolecular interactions among the targeted protein and co-crystallized ligand (ifenprodil) thanks to the ProteinsPlus online server [57], which revealed that Phe176, Glu236 and Gln110 amino acids are the active locations of the targeted protein in its D-chain, as pictured in Figure 5.

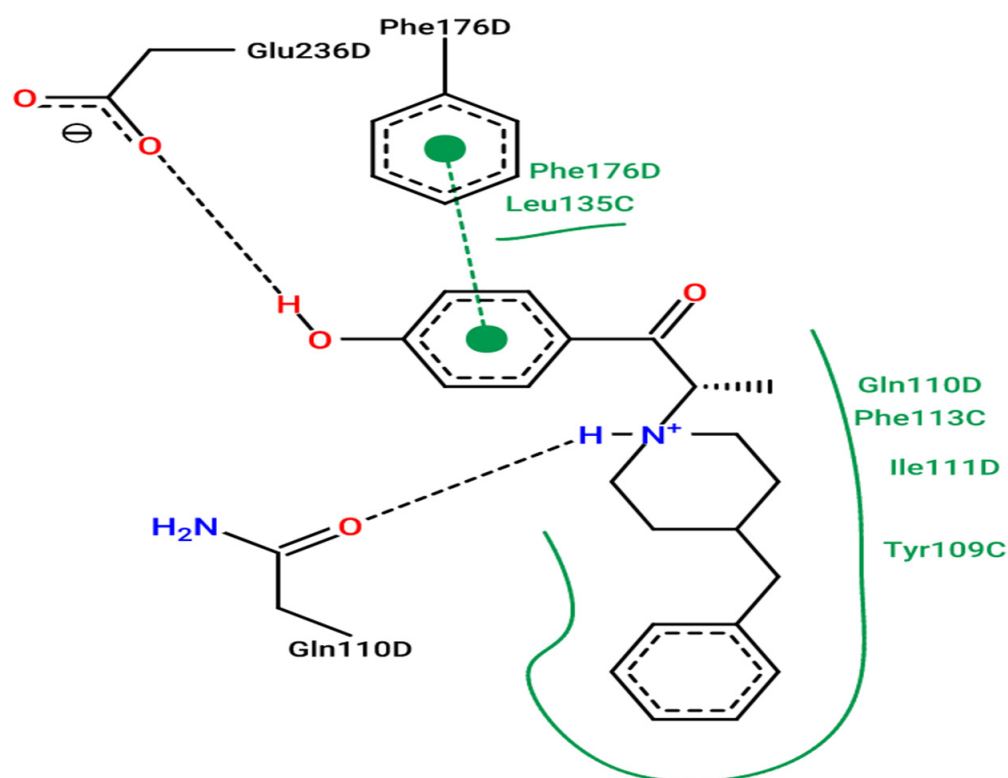


Figure 5. Experimental pose view of ifenprodil with the protein's active sites.

3.6. Docking Validation Protocol

To validate the accuracy of the docking technique, we tested the efficiency of its algorithms, predicting the conformation of the ifenprodil as a co-crystallized ligand by means of the re-docking process, which is mainly based on the overlay of the docked ligand on the ligand attached to the protein in its D chain, as illustrated in Figure 6. Here, 3D (a) and 2D (b) visualizations of chemical interactions established between the docked ifenprodil (binding energy of -5.45 kcal/mol) and the responsible protein prove that Phe176, Glu236 and Gln110 amino acids are similar to those experimentally produced for co-crystallized ifenprodil. Additionally, the superposition result illustrated in Figure 6c reveals a root mean square deviation (RMSD) of 0.395 Å, smaller than 2, which provides an accurate pose prediction. Therefore, the molecular docking protocol is successfully validated [19].

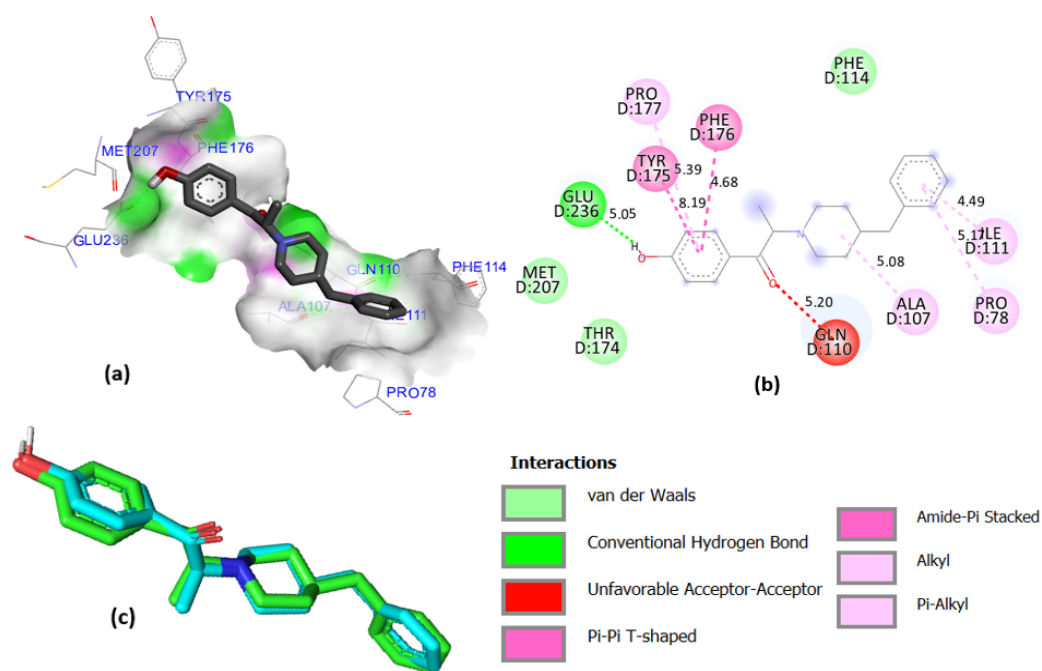
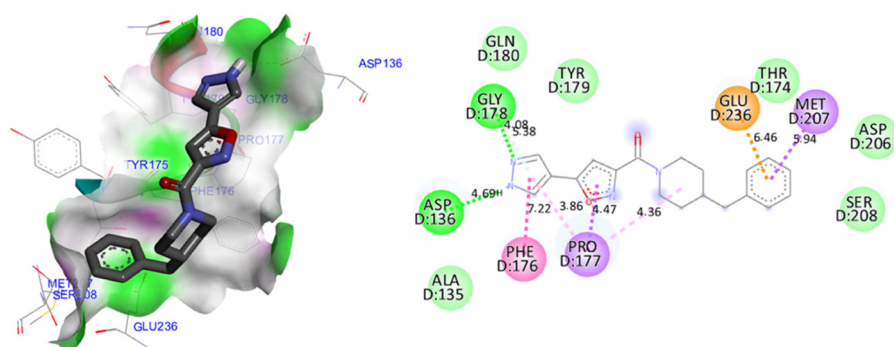


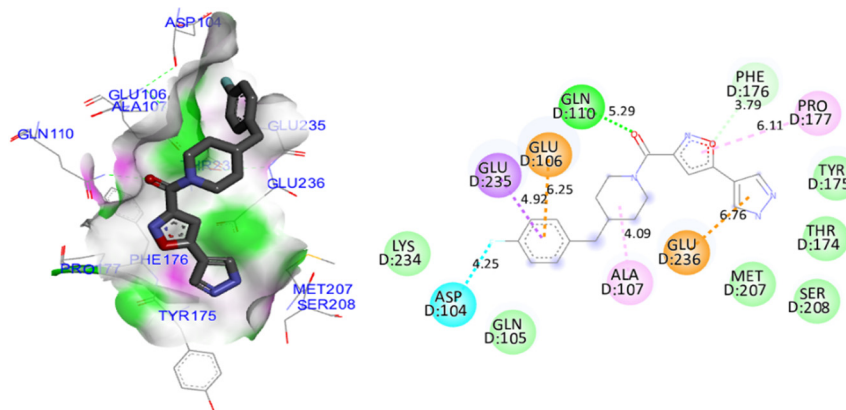
Figure 6. 3D (a) and 2D (b) intermolecular interactions established between the targeted protein and docked ifenprodil with a binding energy equal to -5.45 kcal/mol, and redocking pose (c) with a RMSD value of 0.395 Å (original ifenprodil in cyan, and docked ifenprodil in green).

3.7. Molecular Docking Modeling for L1, L2 and L3 Ligands

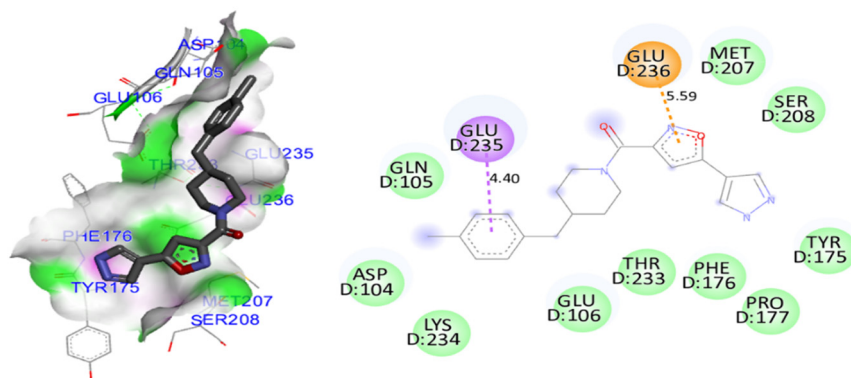
Although the docking protocol was successfully validated, we docked L1, L2 and L3 inhibitors penetrating the blood–brain barrier (BBB) in the same active sites of the protein encoded as 3QEL, and we arrived at the molecular docking results presented in Figure 7. Firstly, the ligand L1 forms two hydrogen bonds, established between Asp136 and Glu178 amino acids and nitrogen atoms of the pyrazole group, with a nuclear distance of 4.69 Å and 4.08 Å, respectively. Moreover, it forms with the same group a chemical bond of amide-pi stacked-type with Phe176 amino acid at a distance of 7.22 Å, in addition to a pi-anion chemical bond with Glu236 amino acid at a nuclear distance of 6.46 Å. Secondly, the ligand L2 forms a hydrogen bond established between the oxygen atom of the acetamide cluster and the Gln110 amino acid, at a nuclear distance of 5.29 Å, as well as a pi-sigma chemical bond with Glu235 amino acid at a distance of 4.92 Å, in addition to a pi-anion chemical bond with Glu236 amino acid at a distance of 6.76 Å, and carbon hydrogen bond linked to the Phe176 amino acid. Thirdly, the ligand L3 forms only two chemical bonds: the first one is a pi-sigma chemical bond created with Glu235 amino acid at a distance of 4.40 Å, and the second one is a pi-anion chemical bond established with Glu236 amino acid, with a nuclear distance of 5.59 Å. Consequently, the results of molecular docking prove that L1, L2 and L3 ligands share a pi-anion chemical bond as a common molecular interaction with Glu236 amino acid. L2 and L3 ligands form a common pi-sigma chemical bond with the Glu235 amino acid. Moreover, both L1 and L2 ligands react with the Phe176 amino acid. As such, compared to the active sites of ifenprodil as a co-crystallized ligand, we conclude that Glu236, Glu235, Gln110, Phe176, Asp136 and Glu178 amino acids are the active sites in which L1, L2 and L3 ligands can inhibit the NMDA receptor subunit 2B, providing analgesic activity against neuropathic pain.



L1–3QEL.pdb complex



L2–3QEL.pdb complex



L3–3QEL.pdb complex

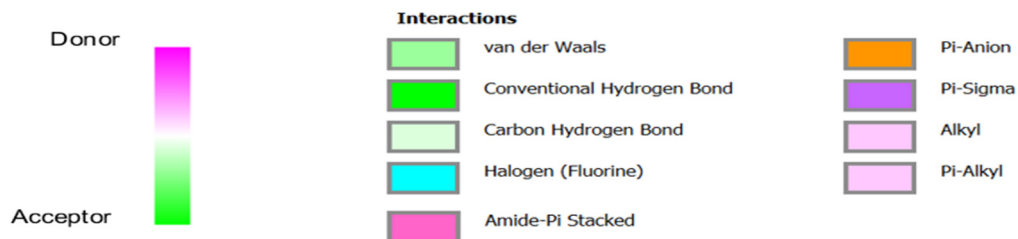


Figure 7. 3D (left) and 2D (right) visualization of intermolecular interactions between L1, L2 and L3 ligands and the transport protein encoded as 3QEL, corresponding to the following binding energies in kcal/mol: −6.45, −5.57 and −6.32, respectively.

4. Conclusions

A systematic in silico study was conducted on a set of thirty-two selective antagonists of N-Methyl-D-Aspartate receptor subunit 2B to identify successful analgesic medications to treat neuropathic pain. Firstly, CoMFA and CoMSIA/EDA models were developed using the 3D-QSAR technique, and were evaluated using internal and external validation, indicating a significant effect of steric, electrostatic and hydrogen bond acceptor fields on the analgesic activity, which is explained through the presence of the [Oxazol-2(3H)-one] group and the halogen-like atomic groups in the meta and para positions of the aromatic cycle of the isoxazole derivatives. Afterwards, in silico ADMET pharmacokinetics prediction demonstrated a desirable profile of L1, L2 and L3 ligands, which were predicted as non-toxic inhibitors for 1A2, 2C19 and 2C9 cytochromes, respecting Lipinski, Veber, Egan, Ghose and Muegge rules, with a high level of absorption that exceeds 89%, and the highest chance of crossing over into the central nervous system (CNS). Finally, the obtained results were further qualified and reinforced using molecular docking simulation, which affirmed that L1, L2 and L3 isoxazoles react specifically with Phe176, Glu235, Glu236, Gln110, Asp136 and Glu178 amino acids of the transport protein encoded as 3QEL. Consequently, they can be applied as therapeutics in the field of medicine to prevent neuropathic diseases. Nevertheless, they need to be exposed to in vitro and in vivo investigations to assess their safety and effectiveness as analgesic medication.

Author Contributions: Conceptualization, M.E.f., M.E. and H.I.; methodology, M.E.f., M.K. and M.E.-r.; software, M.E.f.; validation, S.Z.; data curation, H.I. and S.Z.; writing—original draft preparation, M.E.f. and M.E.-r.; writing—review and editing, H.I., M.E., N.A., O.M.A.k. and A.A.S.; supervision, M.E. All authors have read and agreed to the published version of the manuscript.

Funding: This study was funded by Princess Nourah bint Abdulrahman University Researchers Supporting Project number (PNURSP2022R89), Princess Nourah bint Abdulrahman University, Riyadh, Saudi Arabia.

Institutional Review Board Statement: Not applicable.

Informed Consent Statement: Not applicable.

Data Availability Statement: Not applicable.

Acknowledgments: The authors extend their appreciation to Princess Nourah bint Abdulrahman University Researchers Supporting Project number (PNURSP2022R89), Princess Nourah bint Abdulrahman University, Riyadh, Saudi Arabia for funding this work.

Conflicts of Interest: The authors declare no conflict of interest.

References

1. Bertin, C.; Delage, N.; Rolland, B.; Pennel, L.; Fatseas, M.; Trouvin, A.-P.; Delorme, J.; Chenaf, C.; Authier, N. Analgesic Opioid Use Disorders in Patients with Chronic Non-Cancer Pain: A Holistic Approach for Tailored Management. *Neurosci. Biobehav. Rev.* **2021**, *121*, 160–174. [[CrossRef](#)]
2. Sheikholeslami, M.A.; Ghafghazi, S.; Parvardeh, S.; Koohsari, S.; Aghajani, S.H.; Pouriran, R.; Vaezi, L.A. Analgesic Effects of Cuminal Alcohol (4-Isopropylbenzyl Alcohol), a Monocyclic Terpenoid, in Animal Models of Nociceptive and Neuropathic Pain: Role of Opioid Receptors, L-Arginine/NO/CGMP Pathway, and Inflammatory Cytokines. *Eur. J. Pharmacol.* **2021**, *900*, 174075. [[CrossRef](#)]
3. Noguchi, T.; Umezaki, Y.; Takano, R.; Fujimoto, T.; Domon, Y.; Kubota, K.; Ueda, K.; Kawase, Y.; Yabe, K.; Yokoyama, M.; et al. A Novel [5.2.1]Bicyclic Amine Is a Potent Analgesic without μ Opioid Activity. *Bioorganic Med. Chem. Lett.* **2021**, *36*, 127790. [[CrossRef](#)]
4. Villarreal, Y.R.; Stotts, A.L.; Paniagua, S.M.; Rosen, K.; Eckmann, M.; Suchting, R.; Potter, J.S. Mindfulness Predicts Current Risk of Opioid Analgesic Misuse in Chronic Low Back Pain Patients Receiving Opioid Therapy. *J. Contextual Behav. Sci.* **2020**, *18*, 111–116. [[CrossRef](#)]
5. Wtorek, K.; Piekielna-Ciesielska, J.; Janecki, T.; Janecka, A. The Search for Opioid Analgesics with Limited Tolerance Liability. *Peptides* **2020**, *130*, 170331. [[CrossRef](#)]
6. Arita, T.; Asano, M.; Kubota, K.; Domon, Y.; Machinaga, N.; Shimada, K. Discovery of DS34942424: An Orally Potent Analgesic without Mu Opioid Receptor Agonist Activity. *Bioorganic Med. Chem.* **2020**, *28*, 115714. [[CrossRef](#)]

7. Rossato, M.F.; Oliveira, S.M.; Trevisan, G.; Rotta, M.; Machado, P.; Martins, M.A.P.; Ferreira, J. Structural Improvement of Compounds with Analgesic Activity: AC-MPF4, a Compound with Mixed Anti-Inflammatory and Antinociceptive Activity via Opioid Receptor. *Pharmacol. Biochem. Behav.* **2015**, *129*, 72–78. [CrossRef]
8. Anan, K.; Masui, M.; Tazawa, A.; Tomida, M.; Haga, Y.; Kume, M.; Yamamoto, S.; Shinohara, S.; Tsuji, H.; Shimada, S.; et al. Discovery of NR2B-Selective Antagonists via Scaffold Hopping and Pharmacokinetic Profile Optimization. *Bioorganic Med. Chem. Lett.* **2019**, *29*, 1143–1147. [CrossRef]
9. Temnyakova, N.S.; Vasilenko, D.A.; Barygin, O.I.; Dron, M.Y.; Averina, E.B.; Grishin, Y.K.; Grigoriev, V.V.; Palyulin, V.A.; Fedorov, M.V.; Karlov, D.S. Ifenprodil-like NMDA Receptor Modulator Based on the Biphenyl Scaffold. *Mendeleev Commun.* **2020**, *30*, 342–343. [CrossRef]
10. Wollmuth, L.P.; Chan, K.; Groc, L. The Diverse and Complex Modes of Action of Anti-NMDA Receptor Autoantibodies. *Neuropharmacology* **2021**, *194*, 108624. [CrossRef]
11. Zambre, V.P.; Patil, R.B.; Sangshetti, J.N.; Sawant, S.D. Comprehensive QSAR Studies Reveal Structural Insights into the NR2B Subtype Selective Benzazepine Derivatives as N-Methyl-d-Aspartate Receptor Antagonists. *J. Mol. Struct.* **2019**, *1197*, 617–627. [CrossRef]
12. Lill, M.A. Multi-Dimensional QSAR in Drug Discovery. *Drug Discov. Today* **2007**, *12*, 1013–1017. [CrossRef]
13. Vilar, S.; Cozza, G.; Moro, S. Medicinal Chemistry and the Molecular Operating Environment (MOE): Application of QSAR and Molecular Docking to Drug Discovery. *Curr. Top. Med. Chem.* **2008**, *8*, 1555–1572. [CrossRef]
14. Halder, A.K.; Jha, T. Validated Predictive QSAR Modeling of N-Aryl-Oxazolidinone-5-Carboxamides for Anti-HIV Protease Activity. *Bioorganic Med. Chem. Lett.* **2010**, *20*, 6082–6087. [CrossRef]
15. Roy, K.; Kar, S.; Das, R.N. Validation of QSAR Models. In *Understanding the Basics of QSAR for Applications in Pharmaceutical Sciences and Risk Assessment*; Elsevier: Amsterdam, The Netherlands, 2015; pp. 231–289. ISBN 978-0-12-801505-6.
16. El Mchichi, L.; El Aissouq, A.; Kasmir, R.; Belhassan, A.; El-Mernissi, R.; Ouammou, A.; Lakhlifi, T.; Bouachrine, M. In Silico Design of Novel Pyrazole Derivatives Containing Thiourea Skeleton as Anti-Cancer Agents Using: 3D QSAR, Drug-Likeness Studies, ADMET Prediction and Molecular Docking. *Mater. Today Proc.* **2021**, *45*, 7661–7674. [CrossRef]
17. Bank, R.P.D. RCSB PDB-QEL: Crystal Structure of Amino Terminal Domains of the NMDA Receptor Subunit GluN1 and GluN2B in Complex with Ifenprodil. Available online: <https://www.rcsb.org/structure/3QEL> (accessed on 11 May 2022).
18. Mazigh, M.; El'mbarki, C.; Hadni, H.; Elhallaoui, M. QSAR Studies Combined with DFT-Calculations and Molecular Docking of Polyamine-Sensitive Inhibitors of the NMDA Receptor. *Mediterr. J. Chem.* **2019**, *9*, 164–174. [CrossRef]
19. Abdullahi, M.; Shallangwa, G.A.; Uzairu, A. In Silico QSAR and Molecular Docking Simulation of Some Novel Aryl Sulfonamide Derivatives as Inhibitors of H5N1 Influenza A Virus Subtype. *Beni-Suef Univ. J. Basic Appl. Sci.* **2020**, *9*, 2. [CrossRef]
20. Purcell, W.P.; Singer, J.A. A Brief Review and Table of Semiempirical Parameters Used in the Hueckel Molecular Orbital Method. *J. Chem. Eng. Data* **1967**, *12*, 235–246. [CrossRef]
21. Ghaleb, A.; Aouidate, A.; Bouachrine, M.; Lakhlifi, T.; Sbai, A. In Silico Exploration of Aryl Halides Analogues as CheckpointK-kinase 1 Inhibitors by Using 3D QSAR, Molecular Docking Study, and ADMET Screening. *Adv. Pharm. Bull.* **2019**, *9*, 84–92. [CrossRef]
22. Clark, M.; Cramer, R.D.; Van Opdenbosch, N. Validation of the General Purpose Tripos 5.2 Force Field. *J. Comput. Chem.* **1989**, *10*, 982–1012. [CrossRef]
23. Clark, R.D.; Patterson, D.E.; Bunce, J.D. Comparative Molecular Field Analysis (CoMFA). 1. Effect of Shape on Binding of Steroids to Carrier Proteins. *J. Am. Chem. Soc.* **1988**, *110*, 5959–5967. [CrossRef] [PubMed]
24. Klebe, G.; Abraham, U.; Mietzner, T. Molecular Similarity Indices in a Comparative Analysis (CoMSIA) of Drug Molecules to Correlate and Predict Their Biological Activity. *J. Med. Chem.* **1994**, *37*, 4130–4146. [CrossRef] [PubMed]
25. Stähle, L.; Wold, S. 6 Multivariate Data Analysis and Experimental Design in Biomedical Research. In *Progress in Medicinal Chemistry*; Elsevier: Amsterdam, The Netherlands, 1988; Volume 25, pp. 291–338. ISBN 978-0-444-80965-0.
26. Bush, B.L.; Nachbar, R.B. Sample-Distance Partial Least Squares: PLS Optimized for Many Variables, with Application to CoMFA. *J. Comput. -Aided Mol. Des.* **1993**, *7*, 587–619. [CrossRef] [PubMed]
27. Rosipal, R.; Krämer, N. Overview and Recent Advances in Partial Least Squares. In *Subspace, Latent Structure and Feature Selection*; Lecture Notes in Computer Science; Saunders, C., Grobelnik, M., Gunn, S., Shawe-Taylor, J., Eds.; Springer: Berlin, Heidelberg, 2006; Volume 3940, pp. 34–51. ISBN 978-3-540-34137-6.
28. Polat, E.; Gunay, S. A New Robust Partial Least Squares Regression Method Based on Multivariate MM-Estimators. *Int. J. Math. Stat.* **2017**, *18*, 82–99.
29. Tropsha, A.; Gramatica, P.; Gombar, V. The Importance of Being Earnest: Validation Is the Absolute Essential for Successful Application and Interpretation of QSPR Models. *QSAR Comb. Sci.* **2003**, *22*, 69–77. [CrossRef]
30. Golbraikh, A.; Tropsha, A. Beware of Q²! *J. Mol. Graph. Model.* **2002**, *20*, 269–276. [CrossRef]
31. Baroni, M.; Clementi, S.; Cruciani, G.; Costantino, G.; Riganelli, D.; Oberrauch, E. Predictive Ability of Regression Models. Part II: Selection of the Best Predictive PLS Model. *J. Chemom.* **1992**, *6*, 347–356. [CrossRef]
32. Daoui, O.; Elkhatabi, S.; Chtita, S.; Elkhlabi, R.; Zgou, H.; Benjelloun, A.T. QSAR, Molecular Docking and ADMET Properties in Silico Studies of Novel 4,5,6,7-Tetrahydrobenzo[D]-Thiazol-2-Yl Derivatives Derived from Dimezone as Potent Anti-Tumor Agents through Inhibition of C-Met Receptor Tyrosine Kinase. *Heliyon* **2021**, *7*, e07463. [CrossRef]

33. Ebenezer, O.; Damoyi, N.; Jordaan, M.A.; Shapi, M. Unveiling of Pyrimidindinones as Potential Anti-Norovirus Agents—A Pharmacoinformatic-Based Approach. *Molecules* **2022**, *27*, 380. [CrossRef]
34. Lipinski, C.A.; Lombardo, F.; Dominy, B.W.; Feeney, P.J. Experimental and Computational Approaches to Estimate Solubility and Permeability in Drug Discovery and Development Settings. *Adv. Drug Deliv. Rev.* **1997**, *23*, 3–25. [CrossRef]
35. Veber, D.F.; Johnson, S.R.; Cheng, H.-Y.; Smith, B.R.; Ward, K.W.; Kopple, K.D. Molecular Properties That Influence the Oral Bioavailability of Drug Candidates. *J. Med. Chem.* **2002**, *45*, 2615–2623. [CrossRef] [PubMed]
36. Yalcin, S. Molecular Docking, Drug Likeness, and ADMET Analyses of Passiflora Compounds as P-Glycoprotein (P-Gp) Inhibitor for the Treatment of Cancer. *Curr. Pharmacol. Rep.* **2020**, *6*, 429–440. [CrossRef]
37. Egan, W.J.; Merz, K.M.; Baldwin, J.J. Prediction of Drug Absorption Using Multivariate Statistics. *J. Med. Chem.* **2000**, *43*, 3867–3877. [CrossRef] [PubMed]
38. Egan, W.J.; Lauri, G. Prediction of Intestinal Permeability. *Adv. Drug Deliv. Rev.* **2002**, *54*, 273–289. [CrossRef]
39. Muegge, I.; Heald, S.L.; Brittelli, D. Simple Selection Criteria for Drug-like Chemical Matter. *J. Med. Chem.* **2001**, *44*, 1841–1846. [CrossRef]
40. Gomes, D.; Silvestre, S.; Duarte, A.P.; Venuti, A.; Soares, C.P.; Passarinha, L.; Sousa, Â. In Silico Approaches: A Way to Unveil Novel Therapeutic Drugs for Cervical Cancer Management. *Pharmaceuticals* **2021**, *14*, 741. [CrossRef]
41. Daina, A.; Michielin, O.; Zoete, V. SwissADME: A Free Web Tool to Evaluate Pharmacokinetics, Drug-Likeness and Medicinal Chemistry Friendliness of Small Molecules. *Sci. Rep.* **2017**, *7*, 42717. [CrossRef]
42. PkCSM. Available online: http://biosig.unimelb.edu.au/pkcsm/run_example? (accessed on 8 March 2022).
43. Serrano, A.; Imbernón, B.; Pérez-Sánchez, H.; Cecilia, J.M.; Bueno-Crespo, A.; Abellán, J.L. QN-Docking: An Innovative Molecular Docking Methodology Based on Q-Networks. *Appl. Soft Comput.* **2020**, *96*, 106678. [CrossRef]
44. Berger, M.L.; Maciejewska, D.; Vanden Eynde, J.J.; Mottamal, M.; Żabiński, J.; Kaźmierczak, P.; Rezler, M.; Jarak, I.; Piantanida, I.; Karminski-Zamola, G.; et al. Pentamidine Analogs as Inhibitors of [3H]MK-801 and [3H]Ifenprodil Binding to Rat Brain NMDA Receptors. *Bioorganic Med. Chem.* **2015**, *23*, 4489–4500. [CrossRef]
45. Kouranov, A.; Xie, L.; de la Cruz, J.; Chen, L.; Westbrook, J.; Bourne, P.E.; Berman, H.M. The RCSB PDB Information Portal for Structural Genomics. *Nucleic Acids Research* **2006**, *34*, D302–D305. [CrossRef]
46. *Signals Lead Discovery—Chemical Analytics—PerkinElmer Informatics*; PerkinElmer: Waltham, MA, USA, 2022.
47. Norgan, A.P.; Coffman, P.K.; Kocher, J.-P.A.; Katzmann, D.J.; Sosa, C.P. Multilevel Parallelization of AutoDock 4.2. *J. Cheminform.* **2011**, *3*, 12. [CrossRef] [PubMed]
48. Morris, G.M.; Huey, R.; Lindstrom, W.; Sanner, M.F.; Belew, R.K.; Goodsell, D.S.; Olson, A.J. AutoDock4 and AutoDockTools4: Automated Docking with Selective Receptor Flexibility. *J. Comput. Chem.* **2009**, *30*, 2785–2791. [CrossRef] [PubMed]
49. BIOVIA Discovery Studio-BIOVIA-Dassault Systèmes®. Available online: <https://www.3ds.com/products-services/biovia/products/molecular-modeling-simulation/biovia-discovery-studio/> (accessed on 17 November 2021).
50. El Khatabi, K.; El-mernissi, R.; Aanouz, I.; Ajana, M.A.; Lakhlifi, T.; Shahinozzaman, M.; Bouachrine, M. Benzimidazole Derivatives in Identifying Novel Acetylcholinesterase Inhibitors: A Combination of 3D-QSAR, Docking and Molecular Dynamics Simulation. *Phys. Chem. Res.* **2022**, *10*, 237–249. [CrossRef]
51. Hadni, H.; Elhallaoui, M. 3D-QSAR, Docking and ADMET Properties of Aurone Analogues as Antimalarial Agents. *Heliyon* **2020**, *6*, e03580. [CrossRef] [PubMed]
52. El Fadili, M.; Er-Rajy, M.; Kara, M.; Assouguem, A.; Belhassan, A.; Alotaibi, A.; Mrabti, N.N.; Fidan, H.; Ullah, R.; Ercisli, S.; et al. QSAR, ADMET In Silico Pharmacokinetics, Molecular Docking and Molecular Dynamics Studies of Novel Bicyclo (Aryl Methyl) Benzamides as Potent GlyT1 Inhibitors for the Treatment of Schizophrenia. *Pharmaceuticals* **2022**, *15*, 670. [CrossRef]
53. Daina, A.; Zoete, V. A BOILED-Egg To Predict Gastrointestinal Absorption and Brain Penetration of Small Molecules. *ChemMed-Chem* **2016**, *11*, 1117–1121. [CrossRef]
54. Daina, A.; Michielin, O.; Zoete, V. ILOGP: A Simple, Robust, and Efficient Description of *n*-Octanol/Water Partition Coefficient for Drug Design Using the GB/SA Approach. *J. Chem. Inf. Model.* **2014**, *54*, 3284–3301. [CrossRef]
55. Williams, K. Ifenprodil, a Novel NMDA Receptor Antagonist: Site and Mechanism of Action. *Curr. Drug Targets* **2001**, *2*, 285–298. [CrossRef]
56. Adamski, A.; Kruszka, D.; Dutkiewicz, Z.; Kubicki, M.; Gorczyński, A.; Patroniak, V. Novel Family of Fused Tricyclic [1,4]Diazepines: Design, Synthesis, Crystal Structures and Molecular Docking Studies. *Tetrahedron* **2017**, *73*, 3377–3386. [CrossRef]
57. Zentrum Für Bioinformatik: Universität Hamburg-Proteins Plus Server. Available online: <https://proteins.plus/> (accessed on 8 March 2022).